フェムト・ナノ秒レーザーを用いた非平衡脱離過程の比較研究

王健仲[A]、兼松泰男[A]、 邨次敦[B]、松田冬樹[C]、松田若菜[A]、河井洋輔[A]、豊田岐聡[A]

大阪大学大学院理学研究科物理学専攻[A]、 アトリエ　モノトレム，吹田大阪[B]

京都大学物質－細胞統合システム拠点[C]

Comparative study of Non-Equilibrium Desorption Processes by using Femtosecond and Nanosecond Lasers

J. Z. Wang[A], Y. Kanematsu[A], A. Muratsugu[B], F. Matsuda[C], W. Matsuda[A], Y. Kawai[A] M. Toyoda[A]

Department of Physics, Osaka University[A], Atelier monotrem, Suita Osaka[B]

Institute for Integrated Cell-Material Sciences, Kyoto University[C]

Ultrafast laser interaction with matter triggers various processes depending on the pulse duration and intensity. To investigate the initial non-equilibrium laser desorption/ionization process, we have developed a time-of-flight (TOF) mass spectrometer that uses ultrashort laser pulse as the desorption/ionization source. We compared the TOF spectra obtained by irradiation using nanosecond lasers (ns-laser) and femtosecond lasers (fs-laser), and analyzed with the shifted-Maxwell Boltzmann distribution (SMBD) model and ion trajectory simulations. We performed a laser pulse energy dependent experiment in a range of fs-laser intensities 10^{10}~10^{12} W/cm^2 and observed the emission ion velocity distribution differences. The close match between the experimental ion initial velocity (5400 m/s) and the calculated value (3750 m/s) confirms that acceleration occurred due to electrostatic ablation under fs-laser irradiation. We also observed that the ion signal distribution under fs-laser irradiation exhibits a smaller full width at half maximum (FWHM) compared with ns-laser, which leads to improved mass resolution in mass spectrometry (MS).

Introduction：

Femtosecond lasers (fs-laser) have developed rapidly over the past three decades and opened a wide range of new applications in industry, material science, and mass spectrometry (MS). The fs-laser pulse interaction mechanism with a solid target will be fundamentally different compared to nanosecond laser (ns-laser) pulses because of their ultrashort irradiation periods and ultrahigh intensities [1]. For ns-lasers case, material transformation from a solid surface with a long period and low intensity (10^8–10^9 W/cm^2) pulse proceeds in thermal equilibrium between electrons and local ions, which involves a succession of electron-phonon collisions and energy transfer between ions and lattice of the target material. For the fs-lasers case, the power density is typically between 10^{10} and 10^{16} W/cm^2 [2], and when the laser intensity exceeds the ablation threshold (around 10^{13} to 10^{14} W/cm^2) of the target material, the initial non-equilibrium process within the first 100 fs of laser-matter interaction involves electrostatic ablation: the target surface electrons absorb the pulse energy and escape, creating a strong electrostatic field that pulls out a small number of ions from the target and accelerate ion. After 100 fs, the interaction process proceeds to a transitional state: electron-phonon and electron-ion

collisions occur, and excess laser energy is transferred to the lattice, which causes a large number of ions to be desorbed [3].

When used as desorption/ionization sources with pulsed beams, fs-lasers can be focused on a target material to ablate small amounts of sample, facilitating elemental, isotopic, and classification analysis in MS. In the last twenty years, most studies have focused on high-intensity laser application to improve ion yield efficiency. In preliminary applications of fs-laser desorption/ionization to mass spectrometry imaging (MSI) [4], most research employs an intensity range of 10^{12} to 10^{14} W/cm^2, which typically leads to target surface destruction. Therefore, employing the lowest possible laser intensity is essential to minimize this damage.

We investigated desorption/ionization processes under low-intensity laser conditions, comparing ion kinetic energy differences resulting from ns-laser and fs-laser irradiation. We observed ion acceleration and higher time resolution under femtosecond laser irradiation, in contrast to the quasi-equilibrium ion velocity distribution by nanosecond laser irradiation. Combined with trajectory simulation, we confirmed that ion acceleration occurs as a non-equilibrium process driven by electrostatic ablation.

Electrostatic ablation mechanism:

When a fs-laser is introduced to a solid surface, the laser electric field penetrates a characteristic depth of skin layer l_s because of the skin effect. Within the l_s, laser electric field intensity $E(z)$ decays exponentially as it propagates deeper into the solid $E(z) = E(0)\exp[-z/l_s]$, and electrons absorb the laser energy through inverse bremsstrahlung and resonance absorption, causing the electron's temperature to increase. Through energy conservation law, the electron temperature $T_e(z,t)$ in the skin layer can be expressed as [3,5]

$$T_e(z,t) = \frac{16\pi I_0 t}{3n_e}\exp\left\{-\frac{2z}{l_s}\right\}, \quad (1)$$

here n_e is electron density(cm^{-3}), λ is laser wavelength, and I_0 is the laser intensity (W/cm^2). Once the energy of the electrons reaches the sum of the binding energy (heat of vaporization) ε_b and the work function ε_{esc}, they escape from the solid surface into the vacuum. This process generates a charge separation between the escaped electrons and the remaining ions, leading to the formation of a strong electric field. This electric field accelerates the ions and causes their ejection from the target. The maximum energy of ions dragged from the target reaches [3,5]

$$\varepsilon_i \approx T_e - \varepsilon_{esc} - \varepsilon_b, \quad (2)$$

which can be used to evaluate the ion's kinetic energy.

Ion trajectory simulation:

To analyze the ion signal under different laser parameters, we simulated the potential distribution and ion trajectory depending on the geometry of the acceleration electrode, with the surface charge method [6]. By simulating ion trajectories and calculating their time of flight, the initial velocity distribution of emitted ions can be estimated from the TOF spectrum signal. To further analyze this, we assumed that the emitted ions follow a shifted-Maxwell-Boltzmann distribution (SMBD) [7]

$$f(T_i, v_z) = \left(\frac{m_i}{2\pi k_B T_i}\right)^{\frac{1}{2}} exp\left[-\frac{m_i}{2k_B T_i}\left(v_z - v_{shifted}\right)^2\right], \quad (3)$$

here T_i is ion temperature(K), m_i is mass of the ion, k_B is the Boltzmann constant, v_z is the ion velocity component perpendicular to the target surface, and $v_{shifted}$ is the acceleration term caused by plasma

expansion and electrostatic ablation. This assumption allowed us to simulate the initial ion velocity distributions on the target surface under laser irradiation.

Sample preparation:

Cesium iodide (CsI) has a simple chemical composition; both atomic species are monoisotopic, which simplifies mass spectrometric analyses and is convenient for the study of the physical aspects of the desorption/ionization process [8]. Therefore, we selected the CsI deposit as the sample. CsI was deposited to a thickness of 1000nm under a pressure of 2×10^{-5} Pa, with a deposit velocity of 0.2-0.4 nm/s by using a physical vapor deposition method using the deposit machine (Knenix KVD-670).

Experiment results and discussion:

This study is based on the system setup we developed last year, a TOF mass spectrometer using the ultrashort laser pulse as the desorption/ionization source [9]. We introduced 400 shots each of fs- and ns-laser pulses with energies of 400 nJ (fs-laser: 7.1×10^{11} W/cm^2, ns-laser: 1.3×10^{8} W/cm^2) to ionize deposited CsI and collected the TOF spectrum of Cs^+ ions, as shown in Fig. 1. The deep blue and deep red bars represent the experimental results for fs-laser and ns-laser irradiation, respectively. The peak for the ns-laser case is delayed by approximately 25 ns compared to the fs-laser case. By fitting the results using the SMBD model combined with ion trajectory simulations, we define a fit as achieved when the FWHM and peak position of the simulated TOF spectrum match those of the experimental data. The simulated fs-laser results (light blue bar) show a Cs^+ ion temperature of 1000 K (0.1 eV) with a shifted velocity of 5400 m/s (20.1 eV). The ns-laser simulation (light red bar) shows a Cs^+ temperature of 14,000 K (1.8 eV) and a shifted velocity of 2200 m/s (3.3 eV). These results suggest that fs-laser irradiation induces higher initial ion velocities along the perpendicular axis, indicating an axial acceleration effect, while maintaining lower ion temperatures compared to ns-laser irradiation. We estimated Cs^+ kinetic energy for a fs-laser with 800 nm using Eq. (1) and (2) with n_e=1×10^{22} cm^{-3}(in a unit volume, each CsI molecule provides one electron), ε_{esc} =2.1eV, ε_b =3.3eV [10], and a single pulse duration t=180 fs. We analyzed ion emission kinetic energy from the target surface layer, approaching a depth of $z \to 0$. The calculated Cs^+ kinetic energy ε_i=9.7 eV(3700m/s), which is close to experiment results of $v_{shifted}$=5400 m/s with 20.1 eV kinetic energy.

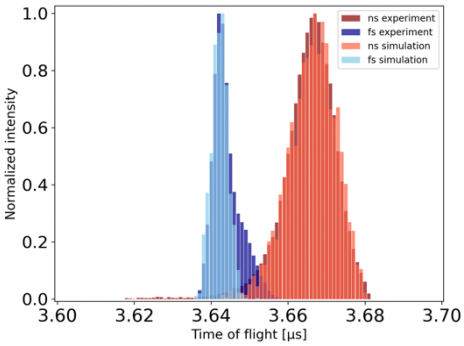

Fig.1. TOF spectra of Cs^+

We increased the pulse energy to investigate the laser intensity dependent in both the fs-laser and ns-laser cases, as shown in Fig. 2. Through ion trajectory simulation, the top x-axis is the initial velocity of Cs^+ fitted to the TOF spectrum. At a pulse energy of 400 nJ, the fs-laser pulse produces a Cs^+ signal distribution with a peak width of 5 ns (FWHM), and the signal peak is located at 3.642 μs, corresponding to an initial velocity of 5.0 km/s. In contrast, under ns-laser irradiation, the FWHM of the peak is 13 ns with an initial velocity of 1.6 km/s. When the pulse energy is increased to 500 nJ, a slight shift in the fs-laser ion TOF spectrum peak to 3.646 μs (4.5 km/s), with an FWHM of 6 ns. The ns-laser ion TOF spectrum peak position remains unchanged at 3.669 μs, but the FWHM broadens to 16 ns. Further increasing to 800

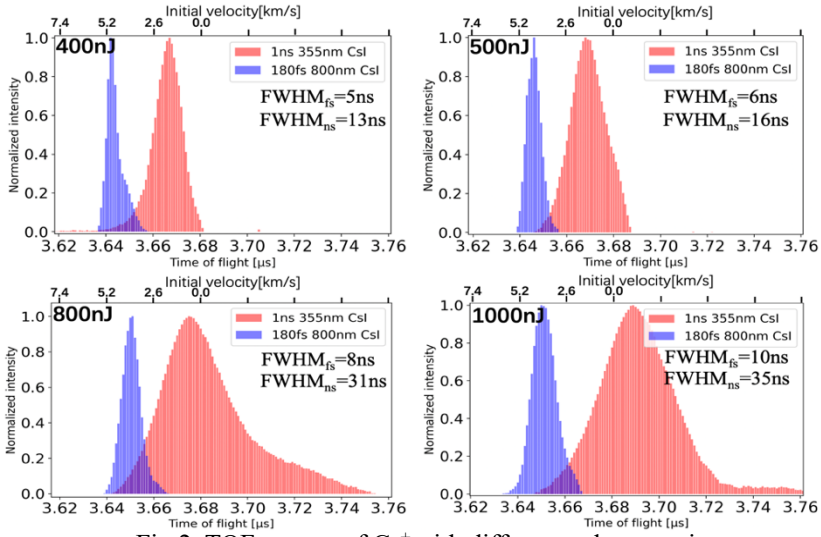

Fig.2. TOF spectra of Cs^+ with different pulse energies

nJ, the fs-laser ion TOF spectrum peak shifted to 3.650 μs (4.0 km/s) with an FWHM of 8 ns, whereas the ns-laser case is 3.675 μs (0.2 km/s), and the FWHM broadens to 31 ns. At a pulse energy of 1000 nJ, the fs-laser TOF spectrum peak remains unchanged, with the FWHM increasing to 10ns. However, the peak velocity of ions under ns-laser irradiation drops below 0 km/s, exhibiting a distinct tail-shape signal distribution. This behavior may be attributed to the sustained emission of ions from the surface for several nanoseconds after the termination of the laser pulse, leading to an FWHM broadening to 35 ns. We could observe as the pulse energy increases, the FWHM of the fs-laser signal broadens slightly, from 5 ns to 10 ns, while the ns-laser FWHM broadens significantly, from 13 ns to 35 ns. Because the lower ion emission temperature (1000K) under the fs-laser, resulting in a narrower SMBD. In contrast, high-temperature (14000K) ions under ns-laser results in a wider initial velocity spread. At the same time, both fs-laser and ns-laser exhibit an ion TOF spectrum peak shift corresponding to slower initial ion velocities. However, this behavior differs from the predictions of Equations (1) and (2), which indicate that electron energy and ion velocity should increase with higher laser intensity. While these equations provide a reasonable energy estimate (in the range of tens of eV), the observed variations in initial ion velocity distribution with fs-laser intensity suggest that the fitting method used here may contribute to this divergence.

Conclusion:

We compared the results of fs-laser and ns-laser irradiation in the low-intensity region using the laser desorption/ionization TOF mass spectrometer which we developed. Through trajectory simulation, it was revealed that fs-lasers possibly induce ion acceleration via electrostatic ablation, resulting in higher ion initial velocities, which closely align with our calculated results. We also found the fs-lasers have an ion signal distribution with a smaller FWHM due to lower ion temperatures, which produced better time resolution in MS. At the same time, ns-lasers generated broader velocity distributions and reduced resolution. It shows the fs-laser's superiority for high-resolution MS.

Reference

[1] L. Jiang *et.al.* Light Sci. Appl. 7 (2018) 17134.
[2] E. Gamaly *et.al.* Prog. Quantum Electron. 37 (2013) 215.
[3] E. Gamaly *et.al.* Phys. Plasmas 9 (2002) 949.
[4] A. V. Walker, Biointerphases, **13**(3), 03B416. (2018)
[5] Rozmus *et.al.* Phys. Rev. A 46 (1992) 7810.
[6] Aoki, J. *et.al.* Nucl. Instrum. Methods Phys. Res. A 600 (2009) 466.
[7] Y. Meng *et.al.* J. Appl. Phys. 89 (2001) 5183.
[8] Fernández-Lima *et.al.* Appl. Surf. Sci. 217 (2003) 202.
[9] 王健仲.第 34 回光物性研究会 (2023) 大阪.
[10] R. Su *et.al.* J. Chem. Phys. 71 (1979) 3194.